A Quantitative Assessment of Nanoparticle−Ligand Distributions: Implications for Targeted Drug and Imaging Delivery in Dendrimer Conjugates

Douglas G. Mullen,[†,‡] Ming Fang,[‡,⊥] Ankur Desai,[‡] James R. Baker, Jr.,[‡] Bradford G. Orr,[‡,§,‖] and Mark M. Banaszak Holl[†,‡,§,⊥,]*

[†]Program in Macromolecular Science and Engineering, [‡]Michigan Nanotechnology Institute for Medicine and Biological Sciences, [§]Program in Applied Physics, [‖]Department of Physics, and [⊥]Department of Chemistry, University of Michigan, Ann Arbor, Michigan 48109

Conjugation strategies commonly employed to attach ligands to the surfaces of nanoparticles generate stochastic distributions of products. Commonly used techniques, including nuclear magnetic resonance (NMR), ultraviolet/visible (UV/vis) spectroscopy, Fourier transformed infrared spectroscopy (FTIR), and elemental analysis, are only capable of determining the mean ligand to nanoparticle ratio and do not provide information about the distribution of species present in the nanomaterial. Other techniques with potential to resolve the distribution of species such as gel permeation chromatography (GPC), high-performance liquid chromatography (HPLC), and matrix-assisted laser desorption ionization time-of-flight (MALDI-TOF) are often unable to do so. The observation of unresolved distributions of macromolecules as "single peaks" using these techniques often leads to optimistic interpretations of sample homogeneity. As such, distributions of nanoparticle−ligand species are not adequately considered in either research studies or systems design. Important questions to ask about the nature of the "average" number of ligands and the distribution from which it arises include:

(1) What are the mean, median, and mode of nanoparticle populations in terms of number of conjugated ligands per particle, and how are they related to each other?

(2) What is the specific number of species that constitutes the observed distributions? What mathematical form best approximates the experimentally observed distribution? Does the mean appropriately represent the material composition?

(3) How does a pre-existing distribution of attachment sites in a population of nanoparticles affect nanoparticle−ligand distributions? This is of particular interest since partial acetylation has been an important step for creating biological functional, targeted PAMAM dendrimers.[1−5] Broadly speaking, this question is relevant to nanoparticle systems that use sequential

ABSTRACT Functional nanoparticles often contain ligands including targeting molecules, fluorophores, and/or active moieties such as drugs. Characterizing the number of these ligands bound to each particle and the distribution of nanoparticle−ligand species is important for understanding the nanomaterial's function. In this study, the amide coupling methods commonly used to conjugate ligands to poly(amidoamine) (PAMAM) dendrimers were examined. A skewed Poisson distribution was observed and quantified using HPLC for two sets of dendrimer−ligand samples prepared using the amine-terminated form of the PAMAM dendrimer and a partially acetylated form of the PAMAM dendrimer that has been used for targeted *in vivo* drug delivery. The prepared samples had an average number of ligands per dendrimer ranging from 0.4 to 13. Distributions identified by HPLC are in excellent agreement with the mean ligand/dendrimer ratio, measured by ^{1}H NMR, gel permeation chromatography (GPC), and potentiometric titration. These results provide insight into the heterogeneity of distributions that are obtained for many classes of nanomaterials to which ligands are conjugated and belie the use of simple cartoon models that present the "average" number of ligands bound as a physically meaningful representation for the material.

KEYWORDS: PAMAM dendrimer · nanotechnology · drug delivery · ligand distribution · nanoparticle characterization

conjugations of different ligands to the same particle.

(4) How does knowledge of the average (mean, median, and mode) and distribution of nanoparticle species affect design and application of nanoparticle−ligand conjugates?

Given the great potential that ligand-conjugated nanomaterials possess with respect to therapeutic delivery,[6−11] cell targeting,[12,13] biomedical diagnostics,[14−17] and sensing,[18,19] a comprehensive understanding of the distributions that result from the conjugation of ligands to nanoparticles is paramount. In this paper, we focus on the distribution of nanoparticle−ligand species that exists for samples produced using poly(amidoamine) (PAMAM) dendrimers and a small molecule ligand. The results from this study are generalizable to a broad range of nanoparticles. Relevant examples include particles composed of gold, iron oxide, polymers, silica, albumin, quantum dots, carbon nanotubes, and dendrimers.[4,5,20−29] This study is most relevant to nanoparticle-based systems produced using stochastic synthesis techniques with an excess of attachment sites on the nanoparticle relative to the number of conjugated ligands, and with the resulting mean number of conjugated ligands ranging from 0.4 to 13. Additionally, this study applies primarily to small and moderate sized ligands relative to the size of the nanoparticle such that site-blocking effects are not introduced by the conjugation of a ligand beyond the single site to which the ligand is covalently linked. This study is therefore less applicable to systems using large ligands such as proteins.[30] A nonexhaustive list of nanoparticle−ligand systems that fit directly in this category include quantum dots conjugated to siRNA,[22] iron oxide nanoparticles conjugated to fluorescein isothiocyanate (FITC)[23] and other small organic molecules,[23,24] and finally, dendrimers conjugated to oligonucleotides,[25,26] folic acid,[4,20,21,27,28] peptides,[5,29] FITC,[29] and other small molecules.[4]

The diversity of ligands that have been conjugated to dendrimers makes the dendrimer a compelling system to study.[31−35] Several of these dendrimer−ligand combinations have been found to be highly effective in biological systems both *in vitro* and *in vivo* with potential to advance to human clinical trials.[2,3,36−41] To facilitate the development of these dendrimer-based nanomaterials into systems with consistent biological activities, it is vital to have knowledge of the distribution of dendrimer−ligand species that compose the material. A final factor making the dendrimer an attractive system to study is that dendrimers are structurally well-defined and well-characterized. This is especially true for PAMAM dendrimers. PAMAM dendrimers have a well-defined branched structure which leads to exceptionally high degrees of monodispersity (PDI = 1.01)

and a quantifiable mean number of surface functional groups. With just two exceptions,[42,43] however, only the mean number of ligands bound per dendrimer has been reported.

The situation is exemplified by the PAMAM dendrimer−ligand system developed for targeted drug delivery by Majoros *et al.*[27] This dendrimer was modified sequentially with a mean of 72 acetyl groups, 4 FITC dye molecules, 4 folic acid (FA) targeting ligands, 60 alcohols from glycidilation, and 5 methotrexate (MTX) drug molecules. Cellular uptake of this targeted nanotherapeutic in epidermal carcinoma (KB) cells was studied by Thomas *et al.*[37] Kukowska-Latallo and co-workers found that the dendrimer-based nanomaterial increased the antitumor activity of MTX and substantially decreased its toxicity relative to the free drug in mice bearing human epithelial cancer tumors.[36] These biological results are very promising, and yet at time of publication, no knowledge existed about the distribution of dendrimer−ligand species that composed the material and gave rise to the observed biological results. For example, the specific number of different G5-FA species that are represented by the mean of 4 FA was not known nor was it known if the largest population was even the dendrimer species with 4 FA molecules. Furthermore, no information existed about how the various ligand distributions were affected by conducting each ligand conjugation reaction in a stepwise fashion with distributions forming in the presence of pre-existing ligand distributions.

In this study, we quantitatively analyze the HPLC traces of two different sets of nanoparticle−ligand samples. The nanoparticle−ligand sets were formed using two different nanoparticles: a G5 PAMAM dendrimer with a mean of 112 primary amines and a partially acetylated G5 PAMAM dendrimer with a mean of 80 Ac and 32 NH_2 groups; and a small molecule ligand: 3-(4-(prop-2-ynyloxy)phenyl)propanoic acid (alkyne ligand). Within each of the two sets (G5-NH_2-alkyne and G5-Ac_{80}-alkyne), samples were synthesized to have ligand means in the range commonly used in dendrimer applications, as well as many other nanoparticle−ligand systems described earlier. The products were analyzed by ^1H NMR spectroscopy to determine the mean ligand−nanoparticle ratio. When combined with GPC and potentiometric titration data, the mean number of ligands per nanoparticle was computed. HPLC combined with a peak fitting method resolved the distribution of dendrimer−ligand species and provided the mean, median, and mode of the number of ligands per particle.

RESULTS

Characterization of the Mean Ligand−Dendrimer Ratio by ^1H NMR Spectroscopy. ^1H NMR spectroscopy can directly measure the number and type of protons present in a sample. In order to obtain peak areas to compare the in-

tegrated ratios of the ligand to dendrimer, it is important to set an appropriate relaxation delay time in the ^{1}H NMR pulse sequence, especially since methyne aromatic protons are being compared to methylene protons. A 10 s delay is sufficient to give quantitative integrations of the ligand/dendrimer ratio. When combined with GPC and potentiometric titration, this ratio was converted to the mean number of ligands per dendrimer in the following manner. The combination of potentiometric titration and number average molecular weight measurements from GPC was used to calculate the mean number of end groups (112 ± 5) per amine-terminated dendrimer (G5-NH$_2$) as described.[4] Experimental characterization of this value rather than using the theoretical value (128) is critical to this process as many defect structures exist in PAMAM dendrimer.[44−46] Next, the ratio of methylene protons on the amine-terminated dendrimer arms (Figure 1a, peaks c and e) to the methyl protons in the acetyl-terminated arms (Figure 1a, peak j) was combined with the total number of end groups per dendrimer to compute the mean number of methyl protons in the partially acetylated dendrimer (240.0). For ligand−dendrimer samples in the partially acetylated dendrimer set (sample E-I), the integrated methyl proton peak was used as the internal reference peak to quantify the mean number of ligands based on integration of the aromatic aa′bb′ pattern proton peaks in the alkyne ligand (Figure 1b).

The number of methyl protons per partially acetylated dendrimer also provided the basis to quantify the mean number of protons in the dendrimer interior. Because the partially acetylated dendrimer was synthesized from the same lot of amine-terminated dendrimer (G5-NH$_2$) as was used in this study for the G5-NH$_2$-based sample set, it was assumed that the number of interior protons was constant for both dendrimer forms (partially acetylated and unacetylated). Thus, the interior proton peaks f, h, and i were used as internal reference peaks to quantify the mean number of conjugated ligands in the G5-NH$_2$ samples (A−D) (Figure 1c).

Table 1 contains the mean number of ligands per dendrimer computed based on the ^{1}H NMR spectroscopic characterization. A comparison of the aa′bb′ proton peaks for samples A−D can be found in Figure 2. As the mean number of ligands per dendrimer increases, the peak full width at half-maximum (fwhm) was observed to increase. A linear fit was obtained (R^2 = 0.98), indicating that the fwhm of the aa′bb′ proton peaks could be used to provide an estimate of the mean number of conjugated ligands (see Supporting Information). A linear relationship was also found between the fwhm and the total number of dendrimer−ligand species present in each sample. This trend was also found for the aa′bb′ proton peaks for samples E−I.
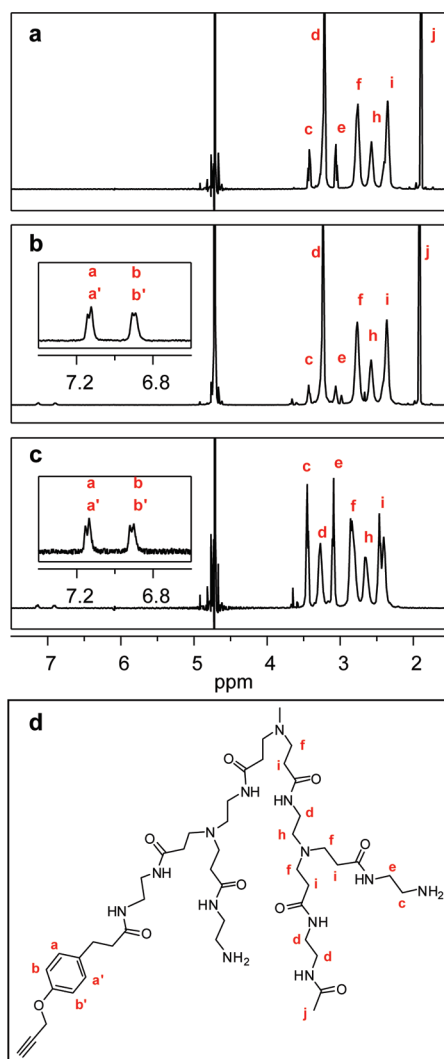

Figure 1. ^{1}H NMR spectra of PAMAM dendrimer conjugates. (a) Spectrum of the partially acetylated dendrimer G5-Ac$_{80}$-(NH$_2$)$_{32}$ **2**. Comparison of peak integrals for the methylene protons (c,e) on primary amine-terminated dendrimer arms with the methyl protons (j) that are unique to acetamide-terminated arms was used to determine the mean ratio of dendrimer arms. Combining this ratio with the mean total number of arms per dendrimer, determined by potentiometric titration and the number average molecular weight measurement from GPC, provides the mean number of amine- and acetamide-terminated arms per dendrimer. These peaks were used as internal reference peaks to determine the mean number of dendrimer interior protons (f,h,i). (b) Spectrum of the partially acetylated dendrimer with a mean of 2.7 alkyne ligands G5-Ac$_{80}$-(NH$_2$)$_{29}$-alkyne$_{2.7}$ (sample G). The mean number of ligands was calculated using the aromatic aa′bb′ proton peaks in the alkyne ligand and the methyl proton peak j. (c) Spectrum of the amine-terminated dendrimer with a mean of 3.8 alkyne ligands G5-(NH$_2$)$_{108}$-alkyne$_{3.8}$ (sample B). The mean number of ligands was calculated using the aromatic aa′bb′ proton peaks in the alkyne ligand and the internal dendrimer proton peaks f, h, and i. (d) Chemical structure and proton labels of four terminal dendrimer arms with three different end group terminations: amine, actyl, amine, and the alkyne ligand (listed right to left).

HPLC Characterization of Dendrimer−Ligand Samples Resolves Distributions of Dendrimer−Ligand Species and Provides the Mean, Median, and Mode. HPLC separates samples based upon their interaction with the stationary phase and

TABLE 1. Comparison of the Average Number of Ligands per Dendrimer Computed by Two Independent Techniques (NMR Spectroscopy and HPLC)

	G5-NH$_2$-alkyne				
	NMR	HPLC			
	arithmetic mean	arithmetic mean	median	mode	no. dendrimer species
sample A	1.1 ± 0.1	0.9 ± 0.04	1	0	6
sample B	3.8 ± 0.4	3.7 ± 0.2	3	3	14
sample C	5.7 ± 0.6	5.8 ± 0.2	5	4	18
sample D	12.9 ± 1.3	13.9 ± 0.6	14	16	27

	G5-Ac$_{80}$-alkyne				
	NMR	HPLC			
	arithmetic mean	arithmetic mean	median	mode	no. dendrimer species
sample E	0.43 ± 0.04	0.4 ± 0.01	0	0	4
sample F	0.7 ± 0.07	0.6 ± 0.02	0	0	5
sample G	2.7 ± 0.3	2.8 ± 0.1	2	1	12
sample H	6.8 ± 0.7	7.2 ± 0.3	7	7	18
sample I	10.2 ± 1.0	11.2 ± 0.5	11	11	24

the eluting solvent. Recently, we have discovered that certain alkyne and azide ligands used for click chemistry also provide excellent tags for separation of the distribution of dendrimer−ligand species using reverse-phase HPLC. Although the dendrimer alone is composed of a number of different structural forms as
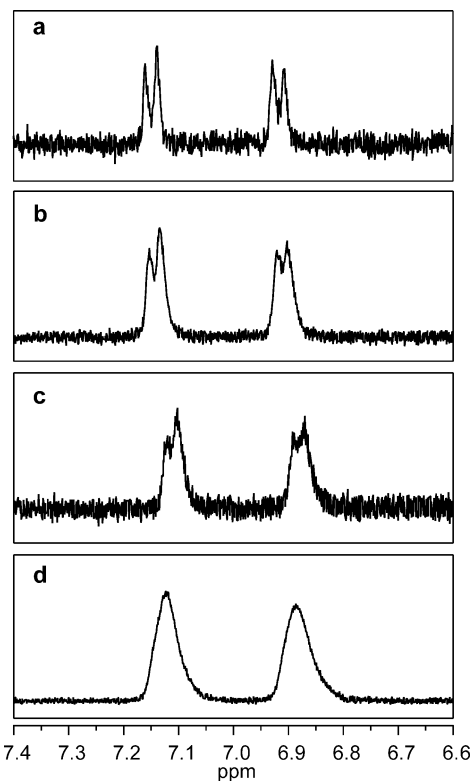

Figure 2. Expanded view of the aa′bb′ proton peaks in the ^{1}H NMR spectra of samples A−D (panels a−d, respectively). As the mean number of ligands increases from 1.1 to 12.9, the full width at half-maximum (fwhm) of both aromatic peaks increases: 13.1, 15.6, 17.3, and 21.3 Hz, respectively.
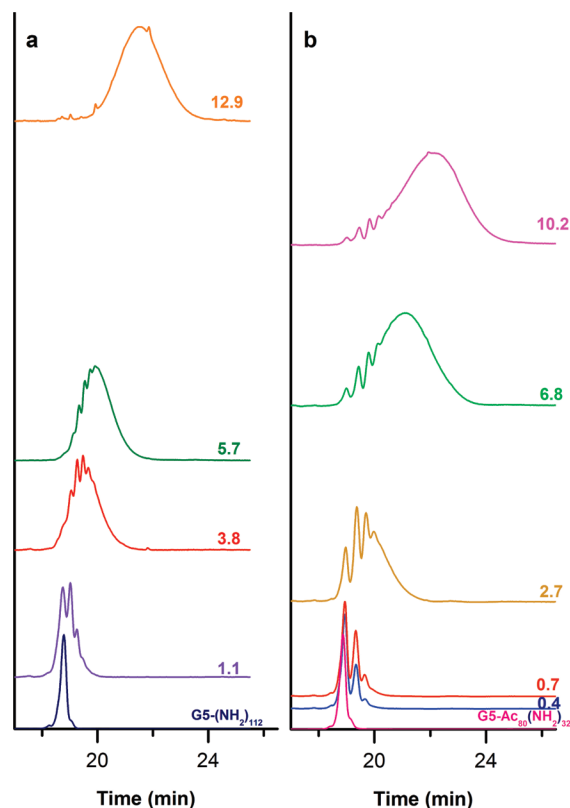

Figure 3. HPLC elution traces of dendrimer−ligand conjugates at 210 nm. Traces were normalized to the largest peak and offset on the vertical axis based on the mean number of ligands per dendrimer. The HPLC trace of the unmodified parent dendrimer for each sample set is provided at the base of each panel (G5-(NH$_2$)$_{112}$ and G5-Ac$_{80}$-(NH$_2$)$_{32}$). (a) HPLC traces for the G5-NH$_2$-alkyne sample set (samples A−D). (b) HPLC traces for the G5-Ac$_{80}$-alkyne sample set (samples E−I).

a result of defects in the polymer backbone, the separation that is achieved using the alkyne and azide ligands is limited to the number of ligands on the different structural forms of the dendrimer. As such, the term "dendrimer−ligand species" in this paper refers to any number of structurally different dendrimers conjugated with a specific number of ligands.

Elution traces of the dendrimer−ligand conjugates were obtained at 210 nm using a C5 reverse-phase column under gradient elution conditions. We have previously shown that 210 nm is a convenient wavelength to monitor PAMAM dendrimers because absorbance is not significantly affected by varying amounts of conjugated ligand and Beer's Law is followed.[42] The traces are grouped in Figure 3 by conjugate type (G5-NH$_2$-alkyne and G5-Ac$_{80}$-alkyne). Traces were baseline corrected, normalized, and plotted on the vertical axis based on each sample's mean number of conjugated ligands. The trace of unmodified dendrimer for each conjugate set (G5-(NH$_2$)$_{112}$ and G5-Ac$_{80}$-(NH$_2$)$_{32}$) is also included.

Two major features were observed in Figure 3. The first feature, found in both conjugate sets, is the trend of increasing trace width as the sample mean increases.
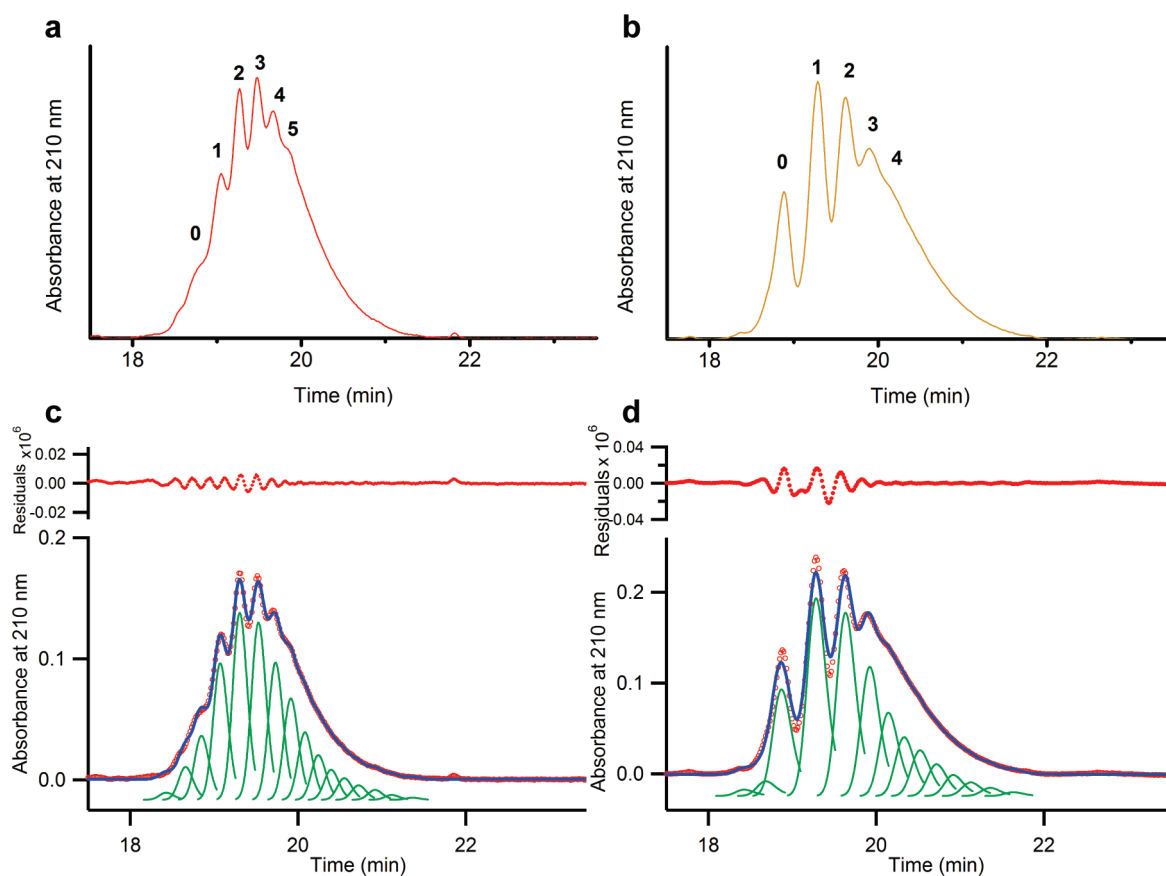
Figure 4. Peak fitting method quantifies the distribution of dendrimer−ligand species resolved in the HPLC elution traces. (a) HPLC trace at 210 nm of sample B (G5-$(NH_2)_{108}$-alkyne$_{3.8}$). Six different peaks (0−5) were observed in the sample's trace. Peak 0 had the same retention time as the parent dendrimer (G5-$(NH_2)_{112}$). (b) HPLC trace at 210 nm of sample G (G5-Ac$_{80}$-$(NH_2)_{109}$-alkyne$_{2.7}$). Five different peaks (0−4) were observed in the sample's trace. Peak 0 had the same retention time as the parent dendrimer (G5-Ac$_{80}$-$(NH_2)_{32}$). (c) Fitted HPLC trace for sample B. The experimental HPLC data are shown with red dots, individual fitting peaks are plotted in green, and the summation of the fitting peaks is plotted in blue. The fitting peak was developed to have the same shape as the parent dendrimer. (d) Fitted HPLC trace for sample G. The color code for panel d is the same as panel c. Residual values for panels c and d are 10^{-6}.

This trend is rather dramatic when one considers the width of the unmodified dendrimer profile. The second feature is the partial resolution of distinct peaks within each trace that have the same peak shape as the unmodified dendrimer. These resolved peaks begin at the same retention time as the unmodified dendrimer and also occur at later retention times.

A comparison between the elution profiles of the G5-NH_2 set and the G5-Ac$_{80}$ set in Figure 3, columns a and b, respectively, reveals several additional observations. Both the trace width and the relative amount of the initially resolved peaks within the sample trace are greater in the G5-Ac$_{80}$-based samples than in the G5-NH_2-based samples with comparable means. The G5-NH_2-based conjugates exhibit a slightly skewed Poissonian profile, whereas the G5-Ac$_{80}$ conjugates show an enhanced skewing. Finally, resolution of the initial peaks in the HPLC traces for the G5-Ac$_{80}$ set is greater compared to the G5-NH_2 set.

Deconvolution of HPLC Traces Using Peak Fitting. Peak fitting analysis provided a means to both identify additional dendrimer−ligand species in the "tailing" region

of the HPLC traces and to quantify the relative concentration of each dendrimer−ligand species in a given sample. A fitting peak for each of the samples was developed by fitting the elution profile of each sample type's unmodified dendrimer (G5-$(NH_2)_{112}$ and G5-Ac$_{80}$-$(NH_2)_{32}$) using Igor Pro 6.01.[42] The functional form employed for the fitting peak was a Gaussian with an exponential decay tail to the right side of the elution peak. Each of the elution profiles for all of the samples in this study was fit with multiple copies of this fitting peak. Figure 4 illustrates this multipeak fitting process with samples B and G. Panels a and b contain each sample's respective HPLC trace. The mean number of ligands for these samples is 3.8 and 2.7, respectively. In Figure 4c,d, the fits for samples B and G are shown with the HPLC trace in red, the multiple copies of the fitting peak in green, and the summation of the fitting peak copies in blue. The position and area of each fitting peak copy were not constrained. Two copies of the fitting peaks were added to the left of peak 0 and constrained in position. These two small peaks were present in the unmodified dendrimer profile and are

likely a result of a small amount of lower generation dendrimer.[47] With the fits for each sample, the relative concentration of each dendrimer−ligand species in the sample was determined.

In both HPLC traces in Figure 4a,b, the first large peak (0) has the same retention time as the unmodified dendrimer: G5-$(NH_2)_{112}$ for panel a and G5-Ac_{80}-$(NH_2)_{32}$ for panel b. The second peak in both panels was preliminarily assigned as being composed of the dendrimer species with exactly 1 ligand (G5-$(NH_2)_{111}$-alkyne$_1$ and G5-Ac_{80}-$(NH_2)_{30}$-alkyne$_1$). It should be noted that, in the naming of these species, the number of alkyne ligands is an exact number while the number of −Ac groups and −NH_2 groups is actually the mean number. The four remaining partially resolved peaks in panel a and three in panel b were assigned to be dendrimer species with sequentially increasing numbers of ligands based on elution order. The additional peaks in the tailing region of the HPLC traces to the left of these partially resolved peaks that were identified by peak fitting (panels c and d) were similarly assigned. Analogous peak assignments were made for all of the dendrimer−ligand samples in this study.

Mean, Median, and Mode of Ligand−Dendrimer Populations Obtained Using HPLC. The relative concentrations of dendrimer species, resolved by HPLC and quantified through the peak fitting analysis, were used to calculate the weighted arithmetic mean of ligands per dendrimer for each sample. This value can be directly compared to the value obtained using ^{1}H NMR spectroscopy (Table 1). For all of samples, the HPLC mean is identical, within error, to the mean determined independently by the combined NMR/GPC/titration analysis. The weighted median and the mode were also determined for each sample.

Distribution Features. Relative concentrations of dendrimer−ligand species for all samples are plotted in Figure 5. These distributions are grouped by sample set (panel a for G5-NH_2-alkyne and panel b for G5-Ac_{80}-alkyne). Three common trends exist across the panels. First, the number of dendrimer−ligand species present in a sample increases as the mean ligand number increases. Second, with the exception of samples D, H, and I, between 8 and 44% of each sample is composed of unmodified dendrimer. In many cases, the unmodified dendrimer is, in fact, the most abundant species present. The third trend, again with the exception of samples D, H, and I, is that the mean dendrimer−ligand species is not identical to the median or mode dendrimer−ligand species.

Additional observations can be made within each of the two sample sets in Figure 5. The G5-NH_2-alkyne samples (Figure 5a) have skewed Poissonian distribution profiles. A close comparison between each of these distributions and a Poisson distribution with the matching mean reveals that the sample distributions have an over-abundance of dendrimer−ligand species at
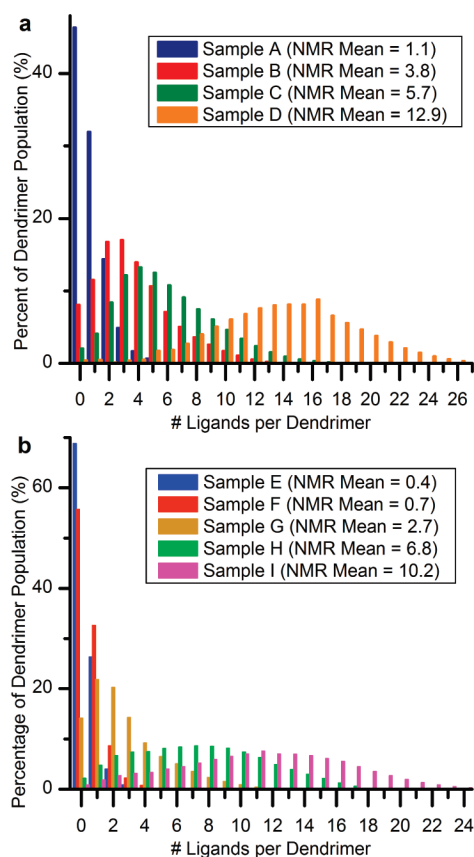

Figure 5. Quantified dendrimer−ligand distributions determined by the peak fitting enabled decovolution of the HPLC traces. (a) Dendrimer−ligand distributions for G5-NH_2-based samples (samples A−D). (b) Dendrimer−ligand distributions for G5-Ac_{80}-$(NH_2)_{32}$-based samples (samples E−I).

both low and high regions of the distribution and an under-abundance of the dendrimer−ligand species with similar numbers of ligands to the sample's mean. The quantified dendrimer−ligand distributions on partially acetylated dendrimer (Figure 5b) exhibit a much more pronounced version of this feature.

Figure 6 provides an additional perspective by grouping the samples based on the sample ligand mean rather than sample set. Panel a contains the two samples with the highest ligand means (10.2 and 12.9). Panel b contains the four samples with medium level ligand means (2.7−6.8). Finally, panel c contains the three samples with the lowest ligand means (0.4−1.1). The initial acylation had a significant effect on the dendrimer−ligand distribution resulting in a significant departure from a pure Poissonian distribution, far greater than was observed for the G5-NH_2-based samples. Also evident in Figure 6 is the greater number of dendrimer−ligand species for the samples that were produced with the partially acetylated dendrimer compared to the G5-NH_2-based sample set.

Distribution Estimations for Folic Acid and Methotrexate-Conjugated Dendrimer. On the basis of the quantified dendrimer−alkyne ligand distributions described
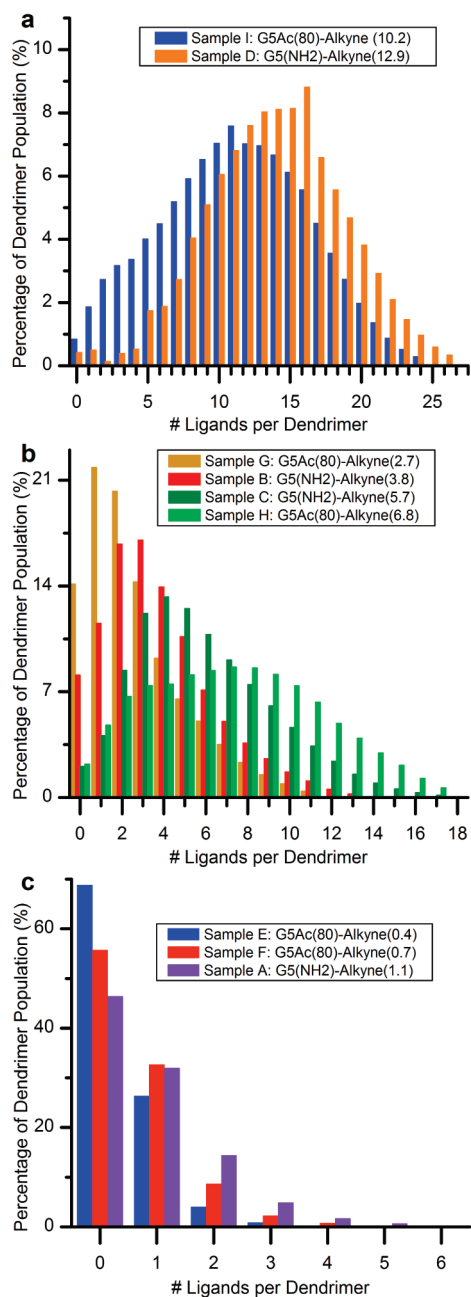
Figure 6. Comparison of dendrimer−ligand distributions for samples with similar ligand means. (a) Distributions for samples I and D with ligand means of 10.2 and 12.9, respectively. (b) Distributions for samples with means between 2.7 and 6.8 (samples G, B, C, and H). (c) Distributions for samples with means between 0.4 and 1.1 (samples E, F, and A).
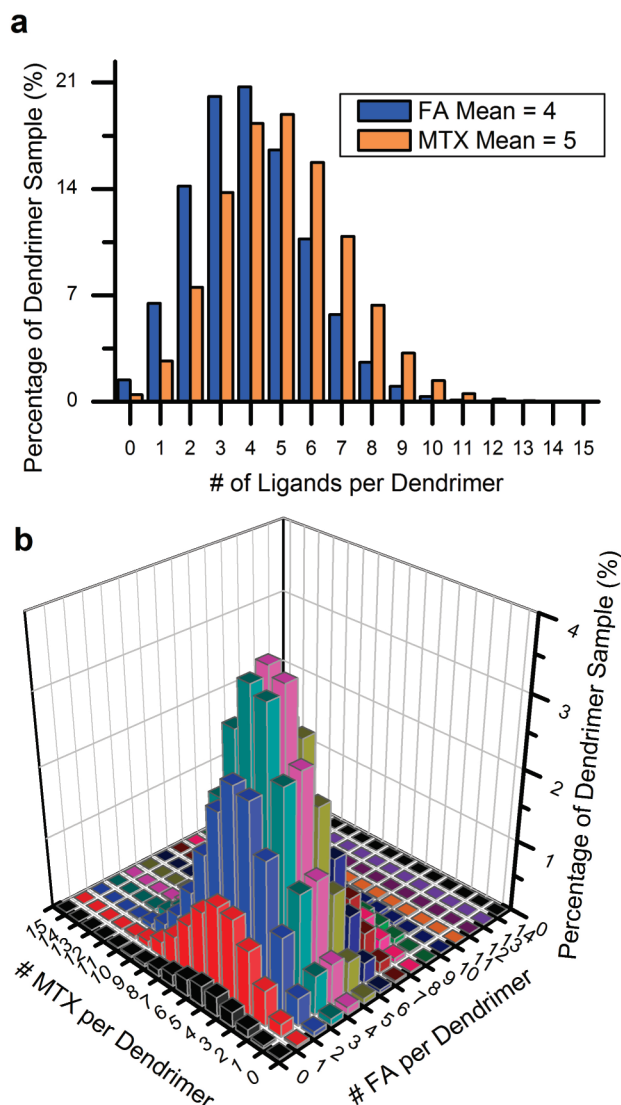

Figure 7. Theoretical distribution of dendrimer species that compose a dendrimer sample with a mean of 4 folic acid and 5 methotrexate molecules per dendrimer. This figure assumes that folic acid and methotrexate follow Poissonian distributions (statistically distributed). (a) Poisson distributions with means of 4 and 5 molecules per dendrimer. (b) Relative concentration of dendrimer species with different numbers of folic acid and methotrexate. Approximately 4% of the dendrimer sample is composed of a dendrimer with exactly 4 folic acid and 5 methotrexate molecules. Only 0.3 to <0.01% is expected to consist 4 folic acid and 5 methotrexate molecules with the optimally active γ regiochemistry.

above, the ligand distributions for the FA- and MTX-conjugated dendrimer, described in the introduction, can be explored. As noted earlier, this particular dendrimer conjugate was determined to have a mean of 4 FA and 5 MTX molecules per dendrimer. Whereas the experimentally determined distributions in this study follow skewed Poissonian functional forms, the mathematical model used for this investigation is a true Poisson model with a prescribed mean and number of available attachment points. Ligand distributions resulting

from this model with means of 4 and 5 representing the FA and MTX ligand distributions are displayed in Figure 7a. Both distributions are combined in a two-dimensional matrix in order to describe all of the different G5-FA-MTX species. The bar plot in Figure 7b contains the sample concentrations for all of the different dendrimer species based on the Poisson distributions for the individual ligands. Approximately 182 (13 × 14) different G5-FA-MTX species are found in this plot. Only 3.9% of the total sample consists of a dendrimer with exactly 4 folic acid and 5 methotrexate molecules. It should be noted that these concentrations assume that the distribution of methotrexate, for example, is not in-

fluenced by the pre-existing distributions of acetyl groups, folic acid molecules and dye molecules that were present during the methotrexate conjugation.

The number of different species in Figure 7b also does not take into account the different regioisomers of folic acid and methotrexate conjugates that have significantly different biological activities. Both compounds have two carboxylic acid groups (α and γ). Several studies have found that folic acid and methotrexate maintain their biological activity when conjugated through the γ-carboxylic acid and either completely lose or experience a substantial reduction in biological activity when conjugated via the α-carboxylic acid.[48−51] The EDC coupling method that is used to conjugate both folic acid and methotrexate to the dendrimer is not regiospecific and results in three different derivatives of both folic acid and methotrexate: amide bond at the γ-position, amide bond at the α-position, and amide bonds at both α- and γ-positions. Taking the three different versions of methotrexate and folic acid into account means that this particular dendrimer system is composed of ∼1638 different dendrimer species. Taking into account folic acid and methotrexate regiochemistry into the consideration of the percentage of sample containing 4 fully active folic acid and 5 fully active methotrexate significantly reduces the estimate from the 3.9% given above. Experimentally determined ratios of γ- versus α-modified forms of folic acid and methotrexate vary from roughly 80 to 30% of the active γ-form relative to the other forms.[48,52,53] The amount of fully active material, when also including the effects of proper regiochemistry, ranges from 0.3% to less than 0.01%.

DISCUSSION

A number of groups have sought to characterize nanoparticle−ligand distributions. Several different methods have been employed including gel electrophoresis,[54] anion-exchange HPLC,[55] ultraperformance liquid chromatography,[43] fluorescence resonance energy transfer,[56] mass spectrometry,[57] and fluorescence quenching.[58] Recently, we published the results of a study that investigated the specific case of dendrimer−ligand conjugates with mean ratios close to 1:1.[42] HPLC was used to resolve the distribution of dendrimer−ligand species, and the peak fitting method was utilized to quantify the different dendrimer−ligand distributions. The observed distributions were found to be consistent with theoretical expectations.

The nature of the distribution of dendrimer−ligand species quantified in this paper suggests that, when possible, investigations of nanoparticle−ligand distributions should be incorporated in all future research studies pertaining to nanoparticle−ligand conjugates, as well as in the design of new generation nanoparticle-based systems. To fully understand the functionality of a nanoparticle−ligand system, knowledge of only the mean ligand/nanoparticle ratio is inadequate. This study provides new information about the relationship between the typically measured average and the actual material composition. Here we seek to address the questions raised earlier in this article.

Relationship between Mean, Median, And Mode. To the best of our knowledge, the average values for all nanoparticle−ligand systems published to date have been arithmetic means. Values for the median and mode have never before been reported. This is a consequence of a reliance on mean-producing characterization techniques and a lack of emphasis on determining the number and relative amount of the different species that gives rise to the mean. Differences between these three forms of the average can be indicative of distribution features. As seen in Table 1, in samples with means of ∼6 or below, the mean, median, and mode can differ substantially. For samples A, E, and F, which all have arithmetic means of 1 or less, the mode of the samples is actually 0. For sample C, which has an arithmetic mean of 6, the mode is actually 4. Also note that for all samples, except D, the mean is always the same or greater than the median and the mode. The significance of considering the various forms of the average value is most apparent when considering samples A and G. In sample A, although the mean is ∼1, the mode is 0. If this ligand was a targeting agent, drug, or dye, the most common species in the dendrimer distribution would have no activity. In sample G, although the mean is ∼3, the mode is 1. If one was designing materials for multivalent targeting, the most common species would exhibit no multivalent binding. For such systems, cartoons that present the mean numbers of ligands are particularly misleading with regards to the biological activity that can be expected.

Dendrimer−Ligand Samples Are Heterogeneous. The dendrimer−ligand distributions that have been quantified in this study contradict the concept that such samples are functionally homogeneous and composed of a relatively small number of constituent species. Although G5 PAMAM dendrimers are, with PDIs as low as 1.01, characterized by high degrees of structural uniformity, this polymeric monodispersity is derived from a synthetic process that exposes a vast molar excess of the monomer unit to the number of attachment points available on the dendrimer. The ligand conjugation reactions to the dendrimer are distinctly different from the dendrimer synthesis because there is instead an excess of attachment points on the dendrimer relative to the molar amount of ligand added. The consequence of this stochastic condition is seen in the number of different dendrimer species for each sample, listed in Table 1. Sample E, with a ligand mean of 0.4, is composed of 4 different dendrimer−ligand species ranging from unmodified dendrimer to dendrimer with 3 ligands. Sample D with the highest mean in this study (12.9)

has 27 different species present ranging from dendrimer with no ligands up to dendrimer with 26 ligands.

The mathematical form that the distributions follow in dendrimer−ligand samples is a skewed Poisson distribution. A comparison of experimentally quantified distributions with Poisson and Gaussian distribution models can be found in Figure 8 for three of the G5-Ac-based samples. The Gaussian comparisons are provided only because many scientists are used to thinking about a distribution of this form and it therefore provides an interesting comparison to the Poisson distribution. In addition, previous work quantifying biotin−dendrimer distributions compared the experimental results to a Gaussian distribution.[29] Panel a displays the distribution for sample H with a mean of 6.8. Three distribution models are included: a Poisson distribution with a mean of 6.8 and 32 available attachment sites, and two Gaussian distributions with means of 6.8 and standard deviations of 1 and 4. Note that the Gaussian with a standard deviation of 1 resembles what one might expect to see in a "homogeneous" sample. This Gaussian distribution does not, however, agree with the heterogeneity observed in the experimental data. In fact, the standard deviation has to be increased to 4 in order to obtain a distribution that resembles sample H. The distribution for sample H is skewed from both the Gaussian with SD = 4 and the Poisson distribution in that there is a systematic over-abundance of species with low and high ligand numbers and an under representation of species with numbers close to the mean. In addition, the skewed Poisson distributions are consistent with our previous results for samples with ligand means of 0.5−1.47.[42]

The heterogeneity observed in these dendrimer−ligand conjugates raises substantial doubt that the mean alone is an adequate measurement to understand nanoparticle−ligand composition and function. As a single value, the mean does not capture the true diversity of species present in the material. Certainly, it is incorrect to infer that the majority of the population is within ±1 ligands of the mean. The only exceptions, in this study, are samples A, E, and F. Note that all of these samples have low mean values (1.1 and lower), below the means typically used for functional dendrimer conjugates. In fact, for samples with ligand means of 6.8 and higher, the majority of dendrimer species present is not even within ±2 ligands of the mean. In addition to this, in many cases, the mean is not the species with the largest relative concentration (the mode). The final problem with relying exclusively on the mean to describe the material composition is that it is completely unable to detect changes in heterogeneity that are caused by differences in the dendrimers' synthetic history (for example, pre-existing distributions).
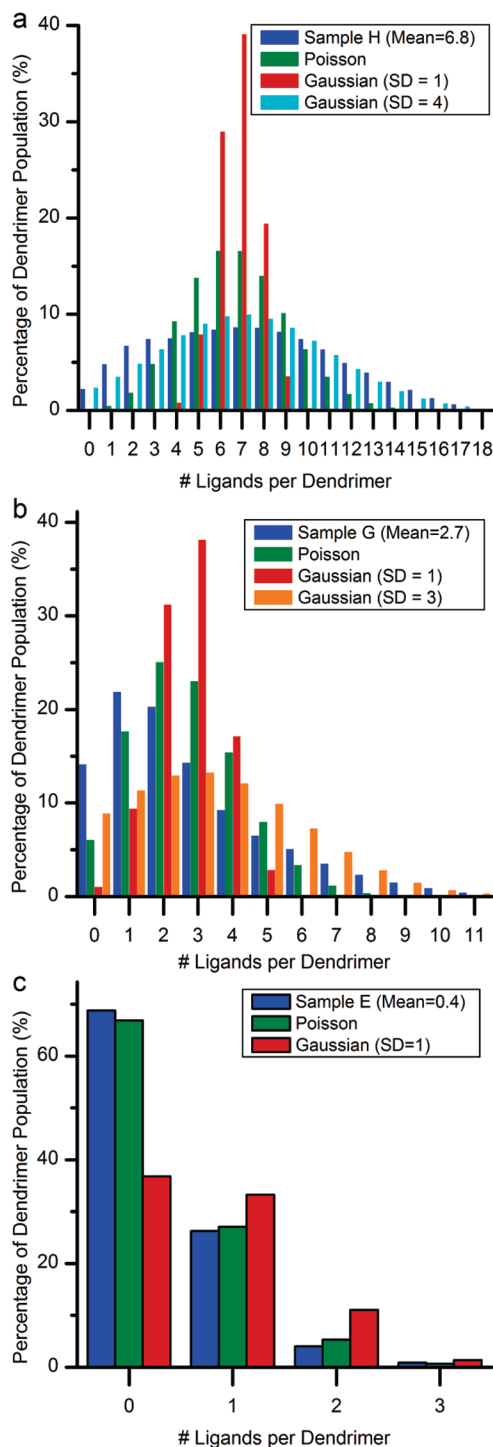

Figure 8. Comparison of dendrimer−ligand distributions with Poisson and Gaussian distributions. In all cases, the Poisson distribution has two inputs: the ligand mean and the total number of available attachment points on the dendrimer surface (32). The Gaussian distribution also has two inputs: the ligand mean and the standard deviation. (a) Distribution for sample H with a mean of 6.8 ligands per dendrimer. Two Gaussian distributions are shown, each with means of 6.8 and with standard deviations of 1 (gold) and 4 (blue). (b) Distribution for sample G with a mean of 2.7 ligands per dendrimer. Two Gaussian distributions are shown, each with means of 2.7 and with standard deviations of 1 (pink) and 3 (green). (c) Distribution for sample E with a mean of 0.4 ligands per dendrimer. The Gaussian distribution has a mean of 0.4 and a standard deviation of 1 (navy).

Pre-existing Distributions Increase Sample Heterogeneity. Many dendrimer−ligand systems employ a partial acylation step before conjugating additional ligands such as FA or MTX. Furthermore, when attaching different ligands, it is common to utilize a sequential reaction strategy. In both of these situations, ligands are conjugated in the presence of a pre-existing distribution making ligand distributions highly sensitive to the nanoparticles' synthetic history.

It is clear from the distribution data that the partially acetylated dendrimer causes an enhanced departure from the slightly skewed Poisson distribution observed in G5-NH$_2$-based samples. Given that the acetylation reaction takes place with an excess of amine groups on the dendrimer relative to the amount of acetic anhydride added, the acetylation reaction itself should result in a distribution composed of dendrimer molecules with different numbers of acetyl groups and consequently a distribution of primary amines for future reactions. The key implication is that the ligand conjugation with the partially acetylated dendrimer takes place in the presence of a pre-existing distribution of primary amines in the dendrimer material. This pre-existing distribution creates a situation wherein dendrimer molecules with high degrees of acetylation have a lower likelihood of reacting with a ligand than the dendrimer molecules in the same sample that have lower degrees of acetylation. The broader implication of this effect is that, when conjugating multiple different functional groups to the dendrimer using conjugation reactions conducted in series, each additional conjugation will experience an increased skewing of the distribution and sample heterogeneity.

In light of the effect that pre-existing distributions have on subsequent ligand conjugations, it is important to point out that the HPLC traces for the two unmodified dendrimer (G5-(NH$_2$) and G5-Ac$_{80}$-(NH$_2$)$_{32}$) are nearly identical. Indeed, the difference in surface amine group heterogeneity between these two samples is not identified by this chromatographic technique. This case should serve as a warning in terms of the problems associated with making conclusions about sample monodispersity based on single peaks.

Implications of Nanoparticle−Ligand Distributions for Understanding Nanoparticle−Ligand Function. This study provides valuable insight into the functional ligand distributions that exist in nanoparticle-based systems, particularly those highlighted in the introduction. For many of these systems, the distribution of nanoparticle−ligand species has not been incorporated into the interpretation of the nanomaterial's biological activity. One particularly relevant example is the multivalent targeting that has been observed for FA-conjugated dendrimer. Previously, Hong and colleagues studied the relationship between multivalent targeting and the mean number of FA per dendrimer using surface plasmon resonance (SPR) and flow cytom-

etry.[59] Five dendrimer samples were generated with means between 2.6 to 13.7. On the basis of the distributions reported earlier in this paper, the dendrimer−folic acid samples were likely composed of between 12 and 27 different species.

In the context of multivalent targeting, consider samples G and H. In sample G, which has a mean of 2.7, approximately 36% of the total dendrimer is not capable of multivalent targeting because it has either 0 or 1 ligand. Approximately 50% of the sample has between 2 and 5 conjugated ligands, which one might reasonably expect to have a multivalent capacity. The 14% of the sample composed of dendrimer with 6 or more ligands may actually be less effective at multivalent targeting both because of a decreased water solubility from the high number of hydrophobic ligand molecules and/or due to ligand−ligand self-aggregation problems.[60] Sample H, with a mean of 6.8, has about 65% of its dendrimer material in this high ligand range. About 29% of the dendrimer population is in the predicted optimal range necessary to achieve multivalency, and about 6% appears incapable of multivalent targeting. This type of analysis can also be applied to multi-ligand systems such as the G5-FA-MTX dendrimer, which would have very complex distributions of its three components (FA, MTX, and acetyl groups). With over 1600 different species, it appears evident that not all species have equal functionalities. In fact, it is very likely that only a small portion of the total material is actually capable of the desired activity. Given the diversity of species in these materials, interpreting biological results based solely on the mean number of functional groups ignores the varying contributions of individual dendrimer species and their concentration relative to the other species present. Incorporating this reality into future studies may lead to significant improvements in nanoparticle−ligand system design, particularly if specific dendrimer species are identified as having significantly enhanced biological activity.

Implications of Distributions for Platform Design. For dendrimer−ligand systems, we propose three modifications to the current multifunctional dendrimer design and synthesis strategy to better control the distribution of dendrimer−ligand species. First, attempts should be made to eliminate the initial partial acetylation of the dendrimer. Although the partially acetylated dendrimer does have the benefit of enhanced solubility in several solvents that are commonly used for functional ligand conjugations, this study demonstrates that skipping this step will lead to a less disperse dendrimer−ligand sample. Second, synthetic strategies that reduce the number of sequential conjugations to the dendrimer should be explored. This could include both combining different functional ligands together before conjugation to the dendrimer, as well as limiting the number of different ligands being conjugated to the dendrimer. Finally, synthetic strategies and separation techniques should be developed that can

reduce the distribution of dendrimer species within a sample.

CONCLUSION

The distributions of dendrimer–ligand species in samples with means between 0.4 and 13 ligands per dendrimer were resolved and quantified using HPLC. The use of partially acetylated dendrimer was found to have a significant effect upon the distribution of dendrimer–ligand species causing a greater skewing from a Poissonian distribution compared to samples prepared using the amine-terminated dendrimer. This suggests that dendrimer–ligand distributions are highly sensitive to the particular dendrimer batch's synthetic history and that these results are applicable to a number of different functional ligands. For the range of dendrimer–ligand samples covered in this study, the average structure does a poor job reflecting the diversity of dendrimer–ligand species that exist in each sample. In many cases, the dendrimer–ligand species with the same number of ligands as the mean number is not even the most abundant species. Knowledge of these distributions for functional nanomaterials can lead to improved system design and predictions of structure, function, and activity of the generated material.

EXPERIMENTAL METHODS

Reagents and Materials. Biomedical grade Generation 5 PAMAM (poly(amidoamine)) dendrimer was purchased from Dendritech Inc. and purified as described in the Synthesis section. MeOH (99.8%), acetic anhydride (99.5%), triethylamine (99.5%), dimethyl sulfoxide (99.9%), dimethylformamide (99.8%), acetone (ACS reagent grade $\geq$99.5%), N,N-diisopropylethylamine, benzotriazol-1-yl-oxytripyrrolidinophosphonium hexafluorophosphate (98%), D_2O, and volumetric solutions (0.1 M HCl and 0.1 M NaOH) for potentiometric titration were purchased from Sigma Aldrich Co. and used as received; 10 000 molecular weight cutoff centrifugal filters (Amicon Ultra) were obtained from Fisher Scientific, and 1× phosphate buffer saline (PBS) (pH = 7.4) without calcium or magnesium was purchased from Invitrogen. The alkyne ligand (3-(4-(prop-2-ynyloxy)phenyl)propanoic acid) was synthesized as described previously.[42]

Nuclear Magnetic Resonance Spectroscopy. All ^{1}H NMR experiments were conducted using a Varian Inova 400 MHz instrument. A 10 s delay time and 64 scans were set for each dendrimer sample. Temperature was controlled at 25 °C. For experiments conducted in D_2O, the internal reference peak was set to 4.717 ppm. Upon measuring T_2* values and empirical studies to ensure that the chosen delay was long enough to avoid any decreased peak intensity associated with spin saturation, the delay for all integration studies was set to 10 s.

Gel Permeation Chromatography. GPC experiments were performed on an Alliance Waters 2695 separation module equipped with a 2487 dual wavelength UV absorbance detector (Waters Corporation), a Wyatt HELEOS Multi Angle Laser Light Scattering (MALLS) detector, and an Optilab rEX differential refractometer (Wyatt Technology Corporation). Columns employed were TosoHaas TSK-Gel Guard PHW 06762 (75 mm × 7.5 mm, 12 μm), G 2000 PW 05761 (300 mm × 7.5 mm, 10 μm), G 3000 PW 05762 (300 mm × 7.5 mm, 10 μm), and G 4000 PW (300 mm × 7.5 mm, 17 μm). Column temperature was maintained at 25 ± 0.1 °C with a Waters temperature control module. The isocratic mobile phase was 0.1 M citric acid and 0.025 wt % sodium azide, pH 2.74, at a flow rate of 1 mL/min. The sample concentration was 10 mg/5 mL with an injection volume of 100 μL. The weight average molecular weight, M_w, was determined by GPC, and the number average molecular weight, M_n, was calculated with Astra 5.3.14 software (Wyatt Technology Corporation) based on the molecular weight distribution.

Reverse-Phase High-Performance Liquid Chromatography. HPLC analysis was carried out on a Waters Delta 600 HPLC system equipped with a Waters 2996 photodiode array detector, a Waters 717 Plus autosampler, and Waters Fraction collector III. The instrument was controlled by Empower 2 software. For analysis of the conjugates, a C5 silica-based RP HPLC column (250 × 4.6 mm, 300 Å) connected to a C5 guard column (4 × 3 mm) was used. The mobile phase for elution of the conjugates was a linear gradient beginning with 100:0 (v/v) water/acetonitrile and ending with 20:80 (v/v) water/acetonitrile over 30 min at a flow rate of 1 mL/min. Trifluoroacetic acid (TFA) at 0.14 wt % concentration in water as well as in acetonitrile was used as a counterion to make the dendrimer surfaces hydrophobic. Elution traces of the dendrimer–ligand conjugate were obtained at 210 nm. We have previously shown that 210 nm is a convenient wavelength to monitor PAMAM dendrimers because absorbance is not significantly affected by varying amounts of conjugated ligand and Beer's Law is followed.[42] Run-to-run reproducibility of retention time was 0.016 min, which is ~4% of the magnitude of the peak-to-peak separation noted in this analysis.

Potentiometric Titration. Potentiometric titration was carried out using a Mettler Toledo MP220 pH meter and a Mettler Toledo In-Lab 430 pH electrode at room temperature, 23 °C. A 10 mL solution of 0.1 N NaCl was added to purified G5 PAMAM dendrimer **1** (127.5 mg) to shield amine group interactions. The pH of the dendrimer solution was lowered to pH = 2.01 using 0.1034 N HCl. A 25 mL Brand Digital Buret III was used for the titration with 0.0987 N NaOH. The numbers of primary and tertiary amines were determined by from the titration curve with NaOH as previously described.[4] (The titration data are provide in the Supporting Information.)

Synthesis. The G5-$(NH_2)_{112}$ dendrimer was conjugated to Ac and alkyne groups. Ac refers to the acetyl termination and alkyne to the alkyne ligand.

Purification of Generation 5 PAMAM Dendrimer G5-$(NH_2)_{112}$. The purchased G5 PAMAM dendrimer was purified by dialysis, as previously described,[42] to remove lower molecular weight impurities including trailing generation dendrimer defect structures. The number average molecular weight (27 100 ± 1000 g/mol) and PDI (1.018 ± 0.014) was determined by GPC. Potentiometric titration was conducted to determine the mean number of primary amines (112 ± 5).

Synthesis of Partially Acetylated Dendrimer G5-Ac_{80}-$(NH_2)_{32}$. Purified G5 PAMAM dendrimer **1** (180.1 mg, 6.588 μmol) was dissolved in anhydrous methanol (26.8 mL). Triethylamine (83.6 μL, 0.600 mmol) was added to this mixture and stirred for 30 min. Acetic anhydride (45.3 μL, 0.480 mmol) was added to anhydrous methanol (7.3 mL), and the resulting mixture was added in a dropwise manner to the dendrimer solution. The reaction was carried out in a glass flask under nitrogen at room temperature for 24 h. Methanol was evaporated from the resulting solution, and the product was purified using 10 000 MWCO centrifugal filtration devices. Purification consisted of six cycles (10 min at 5000 rpm) using 1× PBS (without magnesium and calcium) and six cycles using DI water. The purified dendrimer was lyophilized for 3 days to yield a white solid (124.5 mg, 62%). ^{1}H NMR integration determined the degree of acetylation to be 71.5%.

Synthesis of Dendrimer–Ligand Samples. All reaction steps were carried out in glass scintillation vials at room temperature under nitrogen. All samples were purified using 10 000 MWCO centrifugal filtration devices. Purification consisted of one cycle (10 min at 5000 rpm) using 1× PBS (without magnesium or calcium) and five cycles using DI water.

Samples A–D: G5-NH_2-Alkyne$_{(1.1,3.8,5.7,12.9)}$. Three stock solutions were generated to synthesize samples A–D. A solution of G5

PAMAM dendrimer **1** (37.6 mg, 1.38 μmol) was prepared with anhydrous DMSO (7.000 mL). The alkyne ligand (5.7 mg, 28 μmol) was dissolved in DMSO (2.85 mL). Benzotriazol-1-yl-oxytripyrrolidinophosphonium hexafluorophosphate (PyBOP) (5.5 mg, 10.6 μmol) was dissolved in DMSO (1.10 mL).

Sample A. The alkyne ligand (0.10 mg, 0.49 μmol) solution in anhydrous DMSO (43.9 μL) was added to a solution of G5-NH₂ **1** (8.0 mg, 0.29 μmol) in anhydrous DMSO (1.489 mL). *N,N*-Diisopropylethylamine (0.30 mg, 0.40 μL, 2.3 μmol) was added to the reaction mixture together with 1.091 mL of additional DMSO, and the resulting solution was stirred for 30 min. A solution of PyBOP (0.20 mg, 0.38 μmol) in anhydrous DMSO (44.8 μL) was added in a dropwise manner (0.1 mL/min) to the dendrimer solution. The resulting reaction mixture was stirred for 24 h under nitrogen and then purified as described earlier. The purified product, sample A, was lyophilized for 3 days to yield a white solid (5.7 mg, 71%). ¹H NMR integration determined the mean number of alkyne ligands per dendrimer to be 1.1.

Sample B. Sample B was synthesized in the same manner as sample A, using G5-NH₂ **1** (8.0 mg, 0.29 μmol) in anhydrous DMSO (1.489 mL), the alkyne ligand (0.26 mg, 1.3 μmole) in DMSO (131.8 μL), *N,N*-diisopropylethylamine (1.0 mg, 1.3 μL, 7.5 μmol), 0.913 mL of additional DMSO, and PyBOP (0.70 mg, 1.3 μmol) in anhydrous DMSO (134.4 μL). Sample B was purified and lyophilized in the same manner as sample A. The purified product, sample B, was a white solid (8.0 mg, 97%). ¹H NMR integration determined the mean number of alkyne ligands per dendrimer to be 3.8.

Sample C. Sample C was synthesized in the same manner as sample A, using G5-NH₂ **1** (8.0 mg, 0.29 μmol) in anhydrous DMSO (1.489 mL), the alkyne ligand (0.44 mg, 2.2 μmol) in DMSO (219.7 μL), *N,N*-diisopropylethylamine (1.7 mg, 2.2 μL, 13 μmol), 0.734 mL of additional DMSO, and PyBOP (1.1 mg, 2.2 μmol) in anhydrous DMSO (224.0 μL). Sample C was purified and lyophilized in the same manner as sample A. The purified product, sample C, was a white solid (6.9 mg, 83%). ¹H NMR integration determined the mean number of alkyne ligands per dendrimer to be 5.7.

Sample D. Sample D was synthesized in the same manner as sample A, using G5-NH₂ **1** (8.0 mg, 0.29 μmol) in anhydrous DMSO (1.489 mL), the alkyne ligand (0.88 mg, 4.3 μmol) in DMSO (439.5 μL), *N,N*-diisopropylethylamine (3.3 mg, 4.5 μL, 26 μmol), 0.288 mL of additional DMSO, and PyBOP (2.2 mg, 4.30 μmol) in anhydrous DMSO (447.9 μL). Sample D was purified and lyophilized in the same manner as sample A. The purified product, sample D, was a white solid (8.1 mg, 92%). ¹H NMR integration determined the mean number of alkyne ligands per dendrimer to be 12.9.

Samples E—I: G5-Ac₈₀-Alkyne₍₀.₄,₀.₇,₂.₇,₆.₈,₁₀.₂₎. Three stock solutions were generated to synthesize samples E—I. A solution of the partially acetylated dendrimer **2** (22.4 mg, 0.728 μmol) was prepared with anhydrous DMSO (4.9778 mL). The alkyne ligand (9.9 mg, 49 μmol) was dissolved in DMSO (4.9500 mL). Benzotriazol-1-yl-oxytripyrrolidinophosphonium hexafluorophosphate (Py-BOP) (5.4 mg, 10 μmol) was dissolved in DMSO (1.000 mL).

Sample E. The alkyne ligand (29.0 μg, 0.146 μmol) in anhydrous DMSO (14.6 μL) was added to a solution of partially acetylated dendrimer (4.4 mg, 0.14 μmol) in anhydrous DMSO (0.978 mL). *N,N*-Diisopropylethylamine (1.1 mg, 1.5 μL, 8.6 μmol) was added to the reaction mixture, and the resulting solution was stirred for 30 min. A solution of PyBOP (74.0 μg, 0.143 μmol) in anhydrous DMSO (13.8 μL) was added in a dropwise manner (0.1 mL/min) to the dendrimer solution. The resulting reaction mixture was stirred for 24 h under nitrogen and then purified as described earlier. The purified product, sample E, was lyophilized for 3 days to yield a white solid (3.7 mg, 84%). ¹H NMR integration determined the mean number of alkyne ligands per dendrimer to be 0.4.

Sample F. Sample F was synthesized in the same manner as sample E, using partially acetylated dendrimer (4.4 mg, 0.14 μmol) in anhydrous DMSO (0.978 mL), the alkyne ligand (58.0 μg, 0.286 μmole) in DMSO (29.2 μL), *N,N*-diisopropylethylamine (0.2 mg, 0.3 μL, 2 μmol), and PyBOP (0.15 mg, 0.29 μmol) in anhydrous DMSO (28 μL). Sample F was purified and lyophilized in the same manner as sample E. The purified product, sample F,

was a white solid (3.1 mg, 70%). ¹H NMR integration determined the mean number of alkyne ligands per dendrimer to be 0.7.

Sample G. Sample G was synthesized in the same manner as sample E, using partially acetylated dendrimer (4.4 mg, 0.14 μmol) in anhydrous DMSO (0.978 mL), the alkyne ligand (0.15 mg, 0.72 μmol) in DMSO (73.0 μL), *N,N*-diisopropylethylamine (0.6 mg, 0.7 μL, 4 μmol), and PyBOP (0.37 mg, 0.72 μmole) in anhydrous DMSO (69 μL). Sample G was purified and lyophilized in the same manner as sample E. The purified product, sample G, was a white solid (3.6 mg, 80%). ¹H NMR integration determined the mean number of alkyne ligands per dendrimer to be 2.7.

Sample H. Sample H was synthesized in the same manner as sample E, using partially acetylated dendrimer (4.4 mg, 0.14 μmol) in anhydrous DMSO (0.978 mL), the alkyne ligand (0.29 mg, 1.4 μmol) in DMSO (146 μL), *N,N*-diisopropylethylamine (1.1 mg, 1.5 μL, 8.6 μmol), and PyBOP (0.74 mg, 1.4 μmole) in anhydrous DMSO (138 μL). Sample H was purified and lyophilized in the same manner as sample E. The purified product, sample H, was a white solid (3.5 mg, 76%). ¹H NMR integration determined the mean number of alkyne ligands per dendrimer to be 6.8.

Sample I. Sample I was synthesized in the same manner as sample E, using partially acetylated dendrimer (4.4 mg, 0.14 μmol) in anhydrous DMSO (0.978 mL), the alkyne ligand (0.44 mg, 0.14 μmol) in DMSO (978 μL), *N,N*-diisopropylethylamine (1.7 mg, 2.2 μL, 13 μmol), and PyBOP (1.1 mg, 2.1 μmol) in anhydrous DMSO (207 μL). Sample I was purified and lyophilized in the same manner as sample E. The purified product, sample I, was a white solid (2.7 mg, 57%). ¹H NMR integration determined the mean number of alkyne ligands per dendrimer to be 10.2.

Supporting Information Available: Relationship between the NMR fwhm and the average number of ligands per dendrimer as well as the relationship between the NMR fwhm and the number of different dendrimer—ligand species. This material is available free of charge *via* the Internet at http://pubs.acs.org.

REFERENCES AND NOTES

1. Majoros, I. J.; Keszler, B.; Woehler, S.; Bull, T.; Baker, J. R. Acetylation Of Poly(amidoamine) Dendrimers. *Macromolecules* **2003**, *36*, 5526–5529.
2. Quintana, A.; Raczka, E.; Piehler, L.; Lee, I.; Myc, A.; Majoros, I.; Patri, A. K.; Thomas, T.; Mule, J.; Baker, J. R. Design and Function of a Dendrimer-Based Therapeutic Nanodevice Targeted to Tumor Cells through the Folate Receptor. *Pharm. Res.* **2002**, *19*, 1310–1316.
3. Patri, A. K.; Myc, A.; Beals, J.; Thomas, T. P.; Bander, N. H.; Baker, J. R. Synthesis and *In Vitro* Testing of J591 Antibody—Dendrimer Conjugates for Targeted Prostate Cancer Therapy. *Bioconjugate Chem.* **2004**, *15*, 1174–1181.
4. Majoros, I. J.; Thomas, T. P.; Mehta, C. B.; Baker, J. R. Poly(amidoamine) Dendrimer-Based Multifunctional Engineered Nanodevice for Cancer Therapy. *J. Med. Chem.* **2005**, *48*, 5892–5899.
5. Shukla, R.; Thomas, T. P.; Peters, J.; Kotlyar, A.; Myc, A.; Baker, J. R. Tumor Angiogenic Vasculature Targeting with PAMAM Dendrimer—RGD Conjugates. *Chem. Commun.* **2005**, 5739–5741.
6. Tong, R.; Cheng, J. J. Anticancer Polymeric Nanomedicines. *Polym. Rev.* **2007**, *47*, 345–381.

7. Rawat, M.; Singh, D.; Saraf, S.; Saraf, S. Nanocarriers: Promising Vehicle For Bioactive Drugs. *Biol. Pharm. Bull.* **2006**, *29*, 1790–1798.

8. Patri, A. K.; Majoros, I. J.; Baker, J. R. Dendritic Polymer Macromolecular Carriers for Drug Delivery. *Curr. Opin. Chem. Biol.* **2002**, *6*, 466–471.

9. Peer, D.; Karp, J. M.; Hong, S.; FaroKhzad, O. C.; Margalit, R.; Langer, R. Nanocarriers as an Emerging Platform for Cancer Therapy. *Nat. Nanotechnol.* **2007**, *2*, 751–760.

10. Fortin, J. P.; Wilhelm, C.; Servais, J.; Menager, C.; Bacri, J. C.; Gazeau, F. Size-Sorted Anionic Iron Oxide Nanomagnets as Colloidal Mediators for Magnetic Hyperthermia. *J. Am. Chem. Soc.* **2007**, *129*, 2628–2635.

11. Johns, R. E.; El-Sayed, M. E. H.; Bulmus, V.; Cuschieri, J.; Maier, R.; Hoffman, A. S.; Stayton, P. S. Mechanistic Analysis of Macrophage Response to IRAK-1 Gene Knockdown by a Smart Polymer-Antisense Oligonucleotide Therapeutic. *J. Biomater. Sci., Polym. Ed.* **2008**, *19*, 1333–1346.

12. Josephson, L.; Tung, C. H.; Moore, A.; Weissleder, R. High-Efficiency Intracellular Magnetic Labeling with Novel Superparamagnetic-Tat Peptide Conjugates. *Bioconjugate Chem.* **1999**, *10*, 186–191.

13. Babic, M.; Horak, D.; Trchova, M.; Jendelova, P.; Glogarova, K.; Lesny, P.; Herynek, V.; Hajek, M.; Sykova, E. Poly(L-lysine)-Modified Iron Oxide Nanoparticles for Stem Cell Labeling. *Bioconjugate Chem.* **2008**, *19*, 740–750.

14. Nie, S. M.; Xing, Y.; Kim, G. J.; Simons, J. W. Nanotechnology Applications in Cancer. *Annu. Rev. Biomed. Eng.* **2007**, *9*, 257–288.

15. Landmark, K. J.; DiMaggio, S.; Ward, J.; Kelly, C.; Vogt, S.; Hong, S.; Kotlyar, A.; Myc, A.; Thomas, T. P.; Penner-Hahn, J. E.; Baker, J. R.; Holl, M. M. B.; Orr, B. G. Synthesis, Characterization, and *In Vitro* Testing of Superparamagnetic Iron Oxide Nanoparticles Targeted Using Folic Acid-Conjugated Dendrimers. *ACS Nano* **2008**, *2*, 773–783.

16. Kircher, M. F.; Mahmood, U.; King, R. S.; Weissleder, R.; Josephson, L. A Multimodal Nanoparticle for Preoperative Magnetic Resonance Imaging and Intraoperative Optical Brain Tumor Delineation. *Cancer Res.* **2003**, *63*, 8122–8125.

17. Jain, K. K. Nanotechnology in Clinical Laboratory Diagnostics. *Clin. Chim. Acta* **2005**, *358*, 37–54.

18. Pandana, H.; Aschenbach, K. H.; Gomez, R. D. Systematic Aptamer−Gold Nanoparticle Colorimetry for Protein Detection: Thrombin. *IEEE Sens. J.* **2008**, *8*, 661–666.

19. Park, S. J.; Taton, T. A.; Mirkin, C. A. Array-Based Electrical Detection of DNA with Nanoparticle Probes. *Science* **2002**, *295*, 1503–1506.

20. Myc, A.; Patri, A. K.; Baker, J. R. Dendrimer-Based BH3 Conjugate that Targets Human Carcinoma Cells. *Biomacromolecules* **2007**, *8*, 2986–2989.

21. Chandrasekar, D.; Sistla, R.; Ahmad, F. J.; Khar, R. K.; Diwan, P. V. The Development of Folate-PAMAM Dendrimer Conjugates for Targeted Delivery of Anti-Arthritic Drugs and Their Pharmacokinetics and Biodistribution in Arthritic Rats. *Biomaterials* **2007**, *28*, 504–512.

22. Derfus, A. M.; Chen, A. A.; Min, D. H.; Ruoslahti, E.; Bhatia, S. N. Targeted Quantum Dot Conjugates for SiRNA Delivery. *Bioconjugate Chem.* **2007**, *18*, 1391–1396.

23. Schellenberger, E. A.; Reynolds, F.; Weissleder, R.; Josephson, L. Surface-Functionalized Nanoparticle Library Yields Probes for Apoptotic Cells. *ChemBioChem* **2004**, *5*, 275–279.

24. Polito, L.; Colombo, M.; Monti, D.; Melato, S.; Caneva, E.; Prosperi, D. Resolving the Structure of Ligands Bound to the Surface of Superparamagnetic Iron Oxide Nanoparticles by High-Resolution Magic-Angle Spinning NMR Spectroscopy. *J. Am. Chem. Soc.* **2008**, *130*, 12712–12724.

25. Choi, Y.; Thomas, T.; Kotlyar, A.; Islam, M. T.; Baker, J. R. Synthesis and Functional Evaluation of DNA-Assembled Polyamidoamine Dendrimer Clusters for Cancer Cell-Specific Targeting. *Chem. Biol.* **2005**, *12*, 35–43.

26. Choi, Y. S.; Mecke, A.; Orr, B. G.; Holl, M. M. B.; Baker, J. R. DNA-Directed Synthesis of Generation 7 and 5 PAMAM Dendrimer Nanoclusters. *Nano Lett.* **2004**, *4*, 391–397.

27. Majoros, I. J.; Myc, A.; Thomas, T.; Mehta, C. B.; Baker, J. R. PAMAM Dendrimer-Based Multifunctional Conjugate for Cancer Therapy: Synthesis, Characterization, and Functionality. *Biomacromolecules* **2006**, *7*, 572–579.

28. Chandrasekar, D.; Sistla, R.; Ahmad, F. J.; Khar, R. K.; Diwan, P. V. Folate Coupled Poly(ethyleneglycol) Conjugates of Anionic Poly(amidoamine) Dendrimer for Inflammatory Tissue Specific Drug Delivery. *J. Biomed. Mater. Res., Part A* **2007**, *82A*, 92–103.

29. Hill, E.; Shukla, R.; Park, S. S.; Baker, J. R. Synthetic PAMAM-RGD Conjugates Target and Bind to Odontoblast-like MDPC 23 Cells and the Predentin in Tooth Organ Cultures. *Bioconjugate Chem.* **2007**, *18*, 1756–1762.

30. Aubin-Tam, M. E.; Hamad-Schifferli, K. Structure and Function of Nanoparticle−Protein Conjugates. *Biomed. Mater.* **2008**, *3*, 034001.

31. Cloninger, M. J. Biological Applications of Dendrimers. *Curr. Opin. Chem. Biol.* **2002**, *6*, 742–748.

32. Lee, C. C.; MacKay, J. A.; Frechet, J. M. J.; Szoka, F. C. Designing Dendrimers for Biological Applications. *Nat. Biotechnol.* **2005**, *23*, 1517–1526.

33. Svenson, S.; Tomalia, D. A. Commentary - Dendrimers in Biomedical Applications—Reflections on the Field. *Adv. Drug Delivery Rev.* **2005**, *57*, 2106–2129.

34. Gillies, E. R.; Frechet, J. M. J. Dendrimers and Dendritic Polymers in Drug Delivery. *Drug Discovery Today* **2005**, *10*, 35–43.

35. Wolinsky, J. B.; Grinstaff, M. W. Therapeutic and Diagnostic Applications of Dendrimers for Cancer Treatment. *Adv. Drug Delivery Rev.* **2008**, *60*, 1037–1055.

36. Kukowska-Latallo, J. F.; Candido, K. A.; Cao, Z. Y.; Nigavekar, S. S.; Majoros, I. J.; Thomas, T. P.; Balogh, L. P.; Khan, M. K.; Baker, J. R. Nanoparticle Targeting of Anticancer Drug Improves Therapeutic Response in Animal Model of Human Epithelial Cancer. *Cancer Res.* **2005**, *65*, 5317–5324.

37. Thomas, T. P.; Majoros, I. J.; Kotlyar, A.; Kukowska-Latallo, J. F.; Bielinska, A.; Myc, A.; Baker, J. R. Targeting and Inhibition of Cell Growth by an Engineered Dendritic Nanodevice. *J. Med. Chem.* **2005**, *48*, 3729–3735.

38. Myc, A.; Douce, T. B.; Ahuja, N.; Kotlyar, A.; Kukowska-Latallo, J.; Thomas, T. P.; Baker, J. R. Preclinical Antitumor Efficacy Evaluation of Dendrimer-Based Methotrexate Conjugates. *Anticancer Drugs* **2008**, *19*, 143–149.

39. Baek, M. G.; Roy, R. Synthesis and Protein Binding Properties of T-Antigen Containing Glycopamam Dendrimers. *Bioorg. Med. Chem.* **2002**, *10*, 11–17.

40. Wu, G.; Barth, R. F.; Yang, W. L.; Chatterjee, M.; Tjarks, W.; Ciesielski, M. J.; Fenstermaker, R. A. Site-Specific Conjugation of Boron-Containing Dendrimers to Anti-EGF Receptor Monoclonal Antibody Cetuximab (IMC-C225) and Its Evaluation as a Potential Delivery Agent for Neutron Capture Therapy. *Bioconjugate Chem.* **2004**, *15*, 185–194.

41. Wu, P.; Malkoch, M.; Hunt, J. N.; Vestberg, R.; Kaltgrad, E.; Finn, M. G.; Fokin, V. V.; Sharpless, K. B.; Hawker, C. J. Multivalent, Bifunctional Dendrimers Prepared by Click Chemistry. *Chem. Commun.* **2005**, 5775–5777.

42. Mullen, D. G.; Desai, A. M.; Waddell, J. N.; Cheng, X. M.; Kelly, C. V.; McNerny, D. Q.; Majoros, I. J.; Baker, J. R.; Sander, L. M.; Orr, B. G.; Holl, M. M. B. The Implications of Stochastic Synthesis for the Conjugation of Functional Groups to Nanoparticles. *Bioconjugate Chem.* **2008**, *19*, 1748–1752.

43. Cason, C. A.; Oehrle, S. A.; Fabre, T. A.; Girten, C. D.; Walters, K. A.; Tomalia, D. A.; Haik, K. L.; Bullen, H. A. Improved Methodology for Monitoring Poly(amidoamine) Dendrimers Surface Transformations and Product Quality by Ultra Performance Liquid Chromatography. *J. Nanomaterials* doi: 10.1155/2008/456082.

44. Peterson, J.; Allikmaa, V.; Subbi, J.; Pehk, T.; Lopp, M. Structural Deviations in Poly(amidoamine) Dendrimers: a MALDI-TOF MS Analysis. *Eur. Polym. J.* **2003**, *39*, 33–42.

45. Giordanengo, R.; Mazarin, M.; Wu, J. Y.; Peng, L.; Charles, L. Propagation of Structural Deviations of Poly(amidoamine) Fan-Shape Dendrimers (Generations 0−3) Characterized by MALDI and Electrospray Mass Spectrometry. *Int. J. Mass Spectrom.* **2007**, *266*, 62–75.

46. Tolic, L. P.; Anderson, G. A.; Smith, R. D.; Brothers, H. M.; Spindler, R.; Tomalia, D. A. Electrospray Ionization Fourier Transform Ion Cyclotron Resonance Mass Spectrometric Characterization of High Molecular Mass Starburst (TM) Dendrimers. *Int. J. Mass Spectrom.* **1997**, *165*, 405–418.

47. Shi, X. Y.; Bi, X. D.; Ganser, T. R.; Hong, S. P.; Myc, L. A.; Desai, A.; Holl, M. M. B.; Baker, J. R. HPLC Analysis of Functionalized Poly(amidoamine) Dendrimers and the Interaction between a Folate−Dendrimer Conjugate and Folate Binding Protein. *Analyst* **2006**, *131*, 842–848.

48. Wang, S.; Lee, R. J.; Mathias, C. J.; Green, M. A.; Low, P. S. Synthesis, Purification, and Tumor Cell Uptake of Ga-67-Deferoxamine-Folate, a Potential Radiopharmaceutical for Tumor Imaging. *Bioconjugate Chem.* **1996**, *7*, 56–62.

49. Ke, C. Y.; Mathias, C. J.; Green, M. A. Folate-Receptor-Targeted Radionuclide Imaging Agents. *Adv. Drug Delivery Rev.* **2004**, *56*, 1143–1160.

50. Kralovec, J.; Spencer, G.; Blair, A. H.; Mammen, M.; Singh, M.; Ghose, T. Synthesis of Methotrexate Antibody Conjugates by Regiospecific Coupling and Assessment of Drug and Antitumor Activities. *J. Med. Chem.* **1989**, *32*, 2426–2431.

51. Rosowsky, A.; Forsch, R. A.; Galivan, J.; Susten, S. S.; Freisheim, J. H. Regiospecific Gamma-Conjugation of Methotrexate to Poly(L-lysine)—Chemical and Biological Studies. *Mol. Pharmacol.* **1985**, *27*, 141–147.

52. Wei, W. H.; Fountain, M.; Magda, D.; Wang, Z.; Lecane, P.; Mesfin, M.; Miles, D.; Sessler, J. L. Gadolinium Texaphyrin-Methotrexate Conjugates. Towards Improved Cancer Chemotherapeutic Agents. *Org. Biomol. Chem.* **2005**, *3*, 3290–3296.

53. Mezo, G.; Lang, O.; Jakab, A.; Bai, K. B.; Szabo, I.; Schlosser, G.; Lang, J.; Kohidai, L.; Hudecz, F. Synthesis of Oligotuftsin-Based Branched Oligopeptide Conjugates for Chemotactic Drug Targeting. *J. Pept. Sci.* **2006**, *12*, 328–336.

54. Sperling, R. A.; Pellegrino, T.; Li, J. K.; Chang, W. H.; Parak, W. J. Electrophoretic Separation of Nanoparticles with a Discrete Number of Functional Groups. *Adv. Funct. Mater.* **2006**, *16*, 943–948.

55. Claridge, S. A.; Liang, H. Y. W.; Basu, S. R.; Frechet, J. M. J.; Alivisatos, A. P. Isolation of Discrete Nanoparticle−DNA Conjugates for Plasmonic Applications. *Nano Lett.* **2008**, *8*, 1202–1206.

56. Pons, T.; Medintz, I. L.; Wang, X.; English, D. S.; Mattoussi, H. Solution-Phase Single Quantum Dot Fluorescence Resonance Energy Transfer. *J. Am. Chem. Soc.* **2006**, *128*, 15324–15331.

57. Tracy, J. B.; Kalyuzhny, G.; Crowe, M. C.; Balasubramanian, R.; Choi, J. P.; Murray, R. W. Poly(ethylene glycol) Ligands for High-Resolution Nanoparticle Mass Spectrometry. *J. Am. Chem. Soc.* **2007**, *129*, 6706–6707.

58. Casanova, D.; Giaume, D.; Moreau, M.; Martin, J. L.; Gacoin, T.; Boilot, J. P.; Alexandrou, A. Counting the Number of Proteins Coupled to Single Nanoparticles. *J. Am. Chem. Soc.* **2007**, *129*, 12592–12593.

59. Hong, S.; Leroueil, P. R.; Majoros, I. J.; Orr, B. G.; Baker, J. R.; Holl, M. M. B. The Binding Avidity of a Nanoparticle-Based Multivalent Targeted Drug Delivery Platform. *Chem. Biol.* **2007**, *14*, 107–115.

60. Reddy, J. A.; Abburi, C.; Hofland, H.; Howard, S. J.; Vlahov, I.; Wils, P.; Leamon, C. Folate-Targeted, Cationic Liposome-Mediated Gene Transfer into Disseminated Peritoneal Tumors. *Gene Ther.* **2002**, *9*, 1542–1550.